

Article

Late Mesozoic Granitoid Magmatism in the Evolution of the Eastern Flank of the Mongol-Okhotsk Orogenic Belt (Russia)

Inna M. Derbeko

Institute of Geology and Nature Management, Russian Academy of Sciences, Far Eastern Branch, 675000 Blagoveshchensk, Amur Region, Russia; derbeko@mail.ru

Abstract: In this article, for the first time, a comparison is made of magmatic events that occurred in the northern and southern framing of the eastern flank of the Mongol-Okhotsk orogenic belt. It is established that these events occurred simultaneously. The igneous rocks accompanying these events are identical in their material characteristics. And their geochemical characteristics reflect the geodynamic processes that took place in the frame of the Mongolian-Okhotsk orogenic belt at the end of the Mesozoic. Igneous rocks are represented by a wide range of rocks: from plutonic to volcanic. The range of their material composition is also wide. But the main component belongs to granitoids. At the initial stage of the Late Mesozoic geological events, granitoids of the adakitic series (149–138 Ma) were formed. Then formations of the calc-alkaline series (140–122 Ma) begin to form. However, the rocks of both the first and second stages were formed under suprasubduction conditions. The difference in the composition of these formations is established by the values of Sr-Nd isotopes. This reflects their spatial affiliation. In the northern frame, they break through the widely developed Archean and Proterozoic formations, and in the southern frame, only Proterozoic ones.

Keywords: granitoids; adakites; geochemical characteristics; subduction; Mongol-Okhotsk orogenic belt; Late Mesozoic; synchronous processes



Citation: Derbeko, I.M. Late Mesozoic Granitoid Magmatism in the Evolution of the Eastern Flank of the Mongol-Okhotsk Orogenic Belt (Russia). *Minerals* **2022**, *12*, 1374. <https://doi.org/10.3390/min12111374>

Academic Editor: Hafiz U. Rehman

Received: 27 September 2022

Accepted: 25 October 2022

Published: 28 October 2022

Publisher's Note: MDPI stays neutral with regard to jurisdictional claims in published maps and institutional affiliations.



Copyright: © 2022 by the author. Licensee MDPI, Basel, Switzerland. This article is an open access article distributed under the terms and conditions of the Creative Commons Attribution (CC BY) license (<https://creativecommons.org/licenses/by/4.0/>).

1. Introduction

The Mongol-Okhotsk orogenic belt (MOOB) stretches from Inner Mongolia to the Pacific coast for almost 3000 km (Figure 1a) [1,2]. Its final formation is associated with the closure of the Mongol-Okhotsk Basin (MOB) and marks the completion of the formation of the entire Central Asian Fold Belt as an orogen. The eastern flank of the MOOB in modern schemes is represented by a collage of terranes [2], which were formed as a result of the convergence of the Siberian and North China cratons (Figure 1a) [1,3]. The latter fact served as a justification for the fact that collisional processes played the main role in the formation of the belt. This idea formed the basis of the geodynamic substantiation of all igneous rocks accompanying the evolution of the belt (reviewed in [1]). Although subduction processes in this area were considered by some authors. It was assumed that the Late Carboniferous bilateral subduction occurred under the southern margin of the Siberian craton (Figure 1b) and the Argun superterrane [4]. According to [4], the Early Permian subduction occurred under the Argun–Mamyn massif (Argun superterrane), and at the beginning of the Mesozoic, under the southern framing of the Siberian craton. post-Mesozoic tectonic events have changed the original appearance of MOOB. In the area of the 120th meridian, two cratons approached as close as possible [5] and divided it into the western and eastern flanks (Figure 1b,c). The article deals with the eastern flank of MOOB (EF MOOB). Critical analysis of the existing EF MOOB models is considered in the work of M.L. Parfenov and others [2]. As the most important unresolved issues in the study of the geology of MOOB, the authors identified: (1) the study of the geochemical characteristics of igneous rocks framing the belt, (2) obtaining paleomagnetic characteristics of the formations of the region. Accurate geochronological data [6–12], isotope-geochemical [6–11], and

geophysical observations [13–16] obtained in recent years allow us to take a fresh look at the development of this complex and mineral resource region.

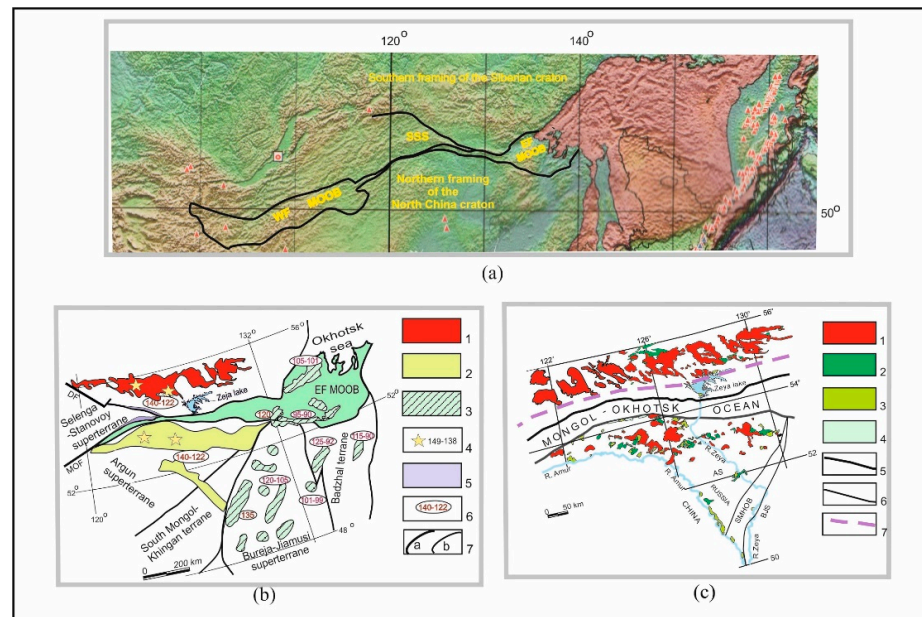


Figure 1. Scheme of the spatial position of the EF MOOB and magmatic complexes in its frame. (a) The position of the MOOB among the regional structures of eastern Asia on the Geological map of the world scale 1:50,000,000 [17]. (b) Scheme of the modern tectonic zoning of the EF MOOB, its framing and the location of the Late Mesozoic magmatic complexes [3], author’s data. The rocks of the suprasubduction (149–122 Ma) and bimodal (119–97 Ma) complexes of the Early Cretaceous in the frame of the EF MOOB (1–2): plutonic ones predominate (1); predominantly volcano-plutonic (2). Late Mesozoic igneous complexes of the eastern end of the MOOB, the Bureya-Jiamusi superterrane, and the Badzhall terrane (3). The area of distribution of adakite granites (4). Melange zones formed in KZ by [5,18] (5). Time of formation of igneous rocks (6). Tectonic boundaries: (a) regional structures; (b) others (6). Fault zone: Dzheltulak (DF), Mongol-Okhotsk (MOF). (c) Scheme of Late Mesozoic tectonic zoning and the location of magmatic formations in its frame before tectonic restructuring in the Cenozoic [5,18]. Igneous rocks (1–3): Late Mesozoic granitoids (149–97 Ma) (1); calc-alkaline volcanic (128–122 Ma) (2); volcanic rocks of the bimodal series (119–97 Ma) (3); trachyandesites, absarokites of rifting (94–88 Ma) (4). Conditional boundary of MOB (5). Structural tectonic boundaries (6). The boundary of the distribution of Late Mesozoic magmatic complexes before tectonic restructuring in the Cenozoic [5] (7). Abbreviation: superterrane-Bureya-Jiamusi (BJS), Argun (AS); South Mongolian-Khinggan Orogenic Belt (SMHOB) [2].

2. Materials and Methods

The article is a generalizing work, in which a comparison of the northern and southern framing of the EF MOOB is carried out. This section describes the methods that were used in the study of igneous rocks in the framing of the EF MOOB. Petrological, geochemical, and isotope-geochemical studies were conducted to determine, which geological events influenced the evolution of the EF MOOB.

2.1. Petrological and Geochemical Studies

In this work, the following laboratory studies were used to substantiate the material characteristics of rocks. To determine the concentrations of the main petrogenic components and elements Sr, Zr, Nb in the studied samples, the X-ray fluorescence method (XRF) was used. These determinations were carried out on a C4 a Pioneer spectrometer in the laboratory of the Institute of Geology and Nature Management of the Far Eastern Branch of the Russian Academy of Sciences (Blagoveshchensk, Russia). Inductively coupled mass

spectrometry (ICP-MS) was used to determine the concentrations of rare and rare-earth elements (REs): (Ga, Ge, Rb, Cs, Sr, Ba, Pb, La, Ce, Pr, Nd, Sm, Eu, Gd, Tb, Dy, Ho, Er, Tm, Yb, Lu, Y, Th, U, Zr, Hf, Nb, Ta, Sc). The study of rocks by this method was carried out at the Institute of Analytical Instrumentation of the Russian Academy of Sciences (St. Petersburg, Russia).

For these studies, the sample was subjected to abrasion. Next, the powder was homogenized by fusing with lithium metaborate (flux) in a muffle furnace at $T = 1150\text{ }^{\circ}\text{C}$. A Pioneer 4S X-ray spectrometer (Bruker, Bremen, Germany) was used for measurements. When determining the intensity values of the analytical lines, the background, absorption, and secondary fluorescence were corrected. The ICP-MS analysis was preceded by sample processing. They were extracted by acid decomposition. PlasmaQuad by VG Elemental was used in the standard mode for measurements. Sensitivity calibration across the entire mass scale was performed using a multi-element REE standard solution manufactured by Matthew Johnson. The relative measurement error corresponds to 3%–10%.

2.2. Isotope-Geochemical Studies

The study of the isotope-geochemical characteristics of rocks was carried out at the Institute of Geology of Ore Deposits, Petrography, Mineralogy and Geochemistry of the Russian Academy of Sciences (Moscow, Russia) under the supervision of A.V. Chugaev.

The isotopic dilution method using mixed tracers ^{85}Rb - ^{84}Sr and ^{149}Sm - ^{150}Nd determined the contents of Rb, Sr, Sm, Nd, as well as the isotope ratios $^{87}\text{Rb}/^{86}\text{Sr}$ and $^{147}\text{Sm}/^{144}\text{Nd}$. Mixed tracers: ^{85}Rb - ^{84}Sr and ^{149}Sm - ^{150}Nd were added to the samples immediately before the chemical decomposition of the samples. To decompose samples, the mass of which varied from 0.1 to 0.2 g (mass samples), the samples were placed in a mixture of concentrated acids HF + HNO₃ (3:1) and kept in a hermetically sealed autoclave at a temperature of about 160 °C until complete dissolution.

To determine the content of Rb, Sr, Sm, and Nd by mass spectrometric analysis, the method of two-stage ion-exchange chromatography was used. The first stage consisted in separating Rb, Sr, and light REE fractions from the matrix elements of the sample. Fractions were isolated in 2.4 M HCl on ion exchange columns filled with 3 mL of BioRad W50x8 cation exchanger (200–400 months). The second stage included the chromatographic separation of Nd and Sm from the rest of the light REE. In this case, columns filled with 0.5 mL of GDEHP ion-exchange resin deposited on Kel-F granules were used. During the chemical preparation of samples for Sr and Nd, the total level of their background contamination did not exceed 0.1 ng.

Mass spectrometric measurements of the isotopic composition of Rb, Sr, Sm, and Nd were carried out on a Sector 54 multi-collector thermal ionization mass spectrometer (Micromass, Great Britain). The accuracy of measurements of the isotope ratios $^{87}\text{Sr}/^{86}\text{Sr}$ and $^{143}\text{Nd}/^{144}\text{Nd}$ was controlled by systematic measurements of the international standard of the Sr isotope composition (SRM-987) and an in-laboratory sample of the Nd isotope composition Nd-IGEM calibrated relative to the international standard LaJolla. The error of the measured ratios $^{87}\text{Sr}/^{86}\text{Sr}$ and $^{143}\text{Nd}/^{144}\text{Nd}$ did not exceed 0.003% ($\pm 2\sigma$ units.). The accuracy of determining the isotopic ratios of $^{87}\text{Sr}/^{86}\text{Sr}$ and $^{147}\text{Sm}/^{144}\text{Nd}$ was 0.5% and 0.2%, respectively ($\pm 2\sigma$ U.).

3. Results

As a result of the research and analysis of literature data, it was established that volcano-plutonic and volcanic complexes were formed in the southern and northern framing of the EF MOOB, starting from the end of the Late Jurassic and were accompanied by various geodynamic settings. Igneous complexes belong to certain structures. In the northern frame, these are the Selengino-Stanovoiy (SSS) and Dzhugdzhur-Stanovoiy (DSS) superterrane, South Mongolian-Khingian Orogenic Belt (SMHOB) (Figure 1b,c). Within the DSS, AS, and SMHOB, rocks of the same composition were formed simultaneously. At the same time, the igneous rocks developed in the SSS and BJS superterrane are asynchronous

to the formation of these complexes both in terms of the time of formation and the material composition of the rocks [1,19,20]. Magmatic formations developed within the DSS, AS, and SMHOB structures were formed almost continuously throughout the Cretaceous. According to the time of their formation and the geodynamic conditions that they accompanied, four stages were distinguished [21–23]: 1, the beginning of subduction (149–138 Ma); 2, the active phase of subduction (140–122 Ma); and 3, the collisional phase (119–97 Ma); 4, destructive processes accompanied by rifting (97–88 Ma). The article considers the first and second stages corresponding to the subduction processes. The third stage is due to the intrusion of bimodal volcano-plutonic complexes and characterizes the completion of the formation of the Mongol-Okhotsk orogen [21]. The fourth stage begins 94 million years ago. This corresponds to the formation of rift structures and intraplate igneous complexes [22].

3.1. Magmatism of the First Stage: 149–38 Ma

Magmatism of the first stage within the DSS, AS, and SMHOB manifested itself at the end of the Jurassic—the beginning of the Early Cretaceous: 149–138 Ma ago. At this stage, adakitic granitoids and volcano-plutonic complexes were formed [23,24]. The rocks of these complexes are not widely distributed. They are represented by subalkaline granites, leucogranites, granites, subalkaline leucogranites, granosyenites and their porphyritic varieties. The rocks of the northern and southern framing of the EF MOOB were formed simultaneously and have a comparable material composition. However, there are differences in isotopic composition due to the material composition of the enclosing rocks.

3.1.1. Magmatism of the First Stage of the Southern Framing EF MOOB

The magmatic formations of the adakite series of the southern framing of the EF MOOB on the territory of AS and SKHOB are represented by rocks of the normal or sub-alkaline series (Figure 2a). These are mainly high-potassium rocks (Figure 2b) of the lime-alkaline series (Figure 2c), at $\text{Na}_2\text{O} + \text{K}_2\text{O} = 7.86\text{--}10.92$ wt.% and $\text{Na}_2\text{O}/\text{K}_2\text{O} = 1.25\text{--}1.81$.

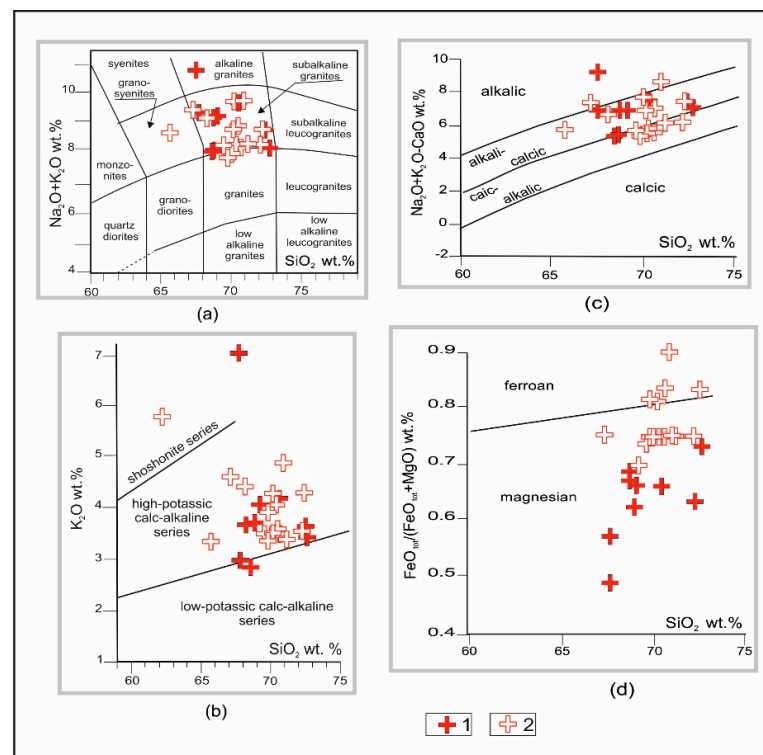


Figure 2. Petrochemical characteristics of adakite series granitoids on classification diagrams: (a) $(\text{Na}_2\text{O} + \text{K}_2\text{O}) - \text{SiO}_2$ [25]; (b) $\text{K}_2\text{O} - \text{SiO}_2$ [26]; (c) $(\text{Na}_2\text{O} + \text{K}_2\text{O} - \text{CaO}) - \text{SiO}_2$ and (d) $\text{FeO}_{\text{tot}}/(\text{FeO}_{\text{tot}} + \text{MgO}) - \text{SiO}_2$ by [27]. Legend: igneous rocks of the southern (1) and northern (2) framing.

The rocks are magnesian (Figure 2d), aluminous at ASI (aluminum saturation index) = 1.06–0.86, which characterizes them as I-type formations [28]. This is also confirmed by the ratios of petrogenic and rare elements (Figure 3a,b).

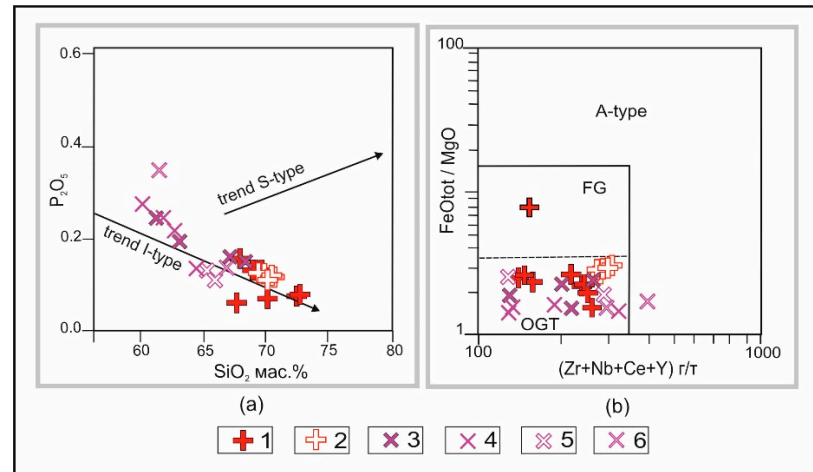


Figure 3. Diagrams for the determination of the petrogeochemical type of granitoids of the EF MOOB framing: (a) P_2O_5/SiO_2 petrochemical type trends by [29]. (b) $FeO_{tot}/MgO - Zr + Nb + Ce + Y$ [30], fields of the rocks: FG-fractionated and OGT-not fractionated M-, I-, S-types; A-type. Legend: granitoids of the adakite series of southern framing (1), of northern framing (2); of the calc-alkaline plutonic series of southern framing (3), of northern framing (4); of the calc-alkaline series hypabyssal of southern framing (5), of northern framing (6).

According to their isotopic and geochemical characteristics, they belong to the negative ϵNd -type with $\epsilon Nd(T) = (-3.3) - (-4.6)$. At the same time, the values of $^{87}Sr/^{86}Sr$ are 0.7069–0.7071 [23]. This indicates the presence of a mantle source. The role of the source, most likely, was to melt the lower continental crust of the Early Proterozoic age (Figure 5). In the southern framing, the outcrops of adakite granitoids are confined to the northern flank of AS (Figure 1b), where the formations of the Karelian and Riphean tiers of the Proterozoic are widely developed [1,3]. A significant volume consists of biotite, garnet–biotite, garnet–bicuspid, kyanite–garnet–biotite, garnet–staurolite–biotite gneisses, as well as hornblende crystal shales with layers of amphibolites.

3.1.2. Magmatism of the First Stage of the Northern Framing EF MOOB

Magmatic formations of the adakite series of the northern framing EF MOOB (DSS) are mainly represented by subalkaline varieties (Figure 2a); granites of the normal series are rare among them. These are predominantly high-potassium formations (Figure 2b) of the calc-alkaline series (Figure 2c), with $Na_2O + K_2O = 7.76–9.78$ wt.%, elevated concentrations of Na_2O (more than 4.4 wt.%) when the ratio of $Na_2O/K_2O = 1.02–1.58$, mainly magnesian (Figure 2d). Glandular varieties are also noted. All rocks represent the aluminous series at $ASI = 0.65–0.74$, which characterizes them as I-type formations [28], confirmed by the ratios of petrogenic and rare elements (Figure 3). A feature of the geochemical composition of the rocks of the northern framing is: elevated concentrations of Sr (up to 1.900 ppm), Ba (up to 2.750 ppm); partially elevated-Rb (up to 73 ppm), Th (up to 14 ppm); at low concentrations of Nb (4.0–11.0 ppm), Ta (0.4–0.6 ppm) and abnormally low concentrations of HREEs (in ppm): Tb (0.11–0.35), Dy (0.4–2.5), Ho (0.08–0.40); Er (0.22–0.68); Tm (0.03–0.09); Lu (0.02–0.09), as well as Y (1.6–11) and Yb (0.02–0.09). In the adakite granitoids of the northern framing, rare earth reveals a stronger fractionation: $(La/Yb) n = 22–110$. They also show a positive Eu anomaly or its absence: $(Eu/Eu^*) n = 0.78–1.49$ (Figure 4). According to the isotope-geochemical characteristics, granitoids belong to the negative ϵNd -type with $\epsilon Nd(T) = (-8.5, -15.47, -14.0, -11.48)$, with changing data, $TNd(DM-2st)$ from 2.5–1.9 bln.

years [8–10], unpublished data of the author. The values of $^{87}\text{Sr}/^{86}\text{Sr}$ are 0.7071–0.7072 [10]. This indicates the presence of a mantle source; which role may have been in the melting of the lower continental crust of the Early Proterozoic age with an inclusion of the Archean crustal component. This fact is illustrated by the diagram of the ratio of primary isotopic Sr and Nd compositions (Figure 5).

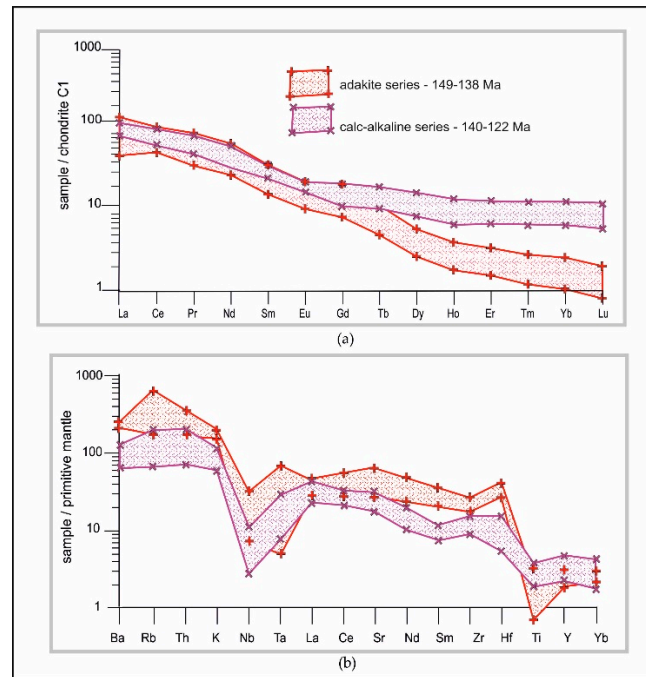


Figure 4. Concentrations of the rare elements in the granitoids of the EF MOOB framing standardized to the composition of Chondrite (a) and primitive mantle (b). Compositions of chondrite C1 and primitive mantle are brought according to the data [31]. Symbols of granitoids: adakite series (1), calc-alkaline series (2).

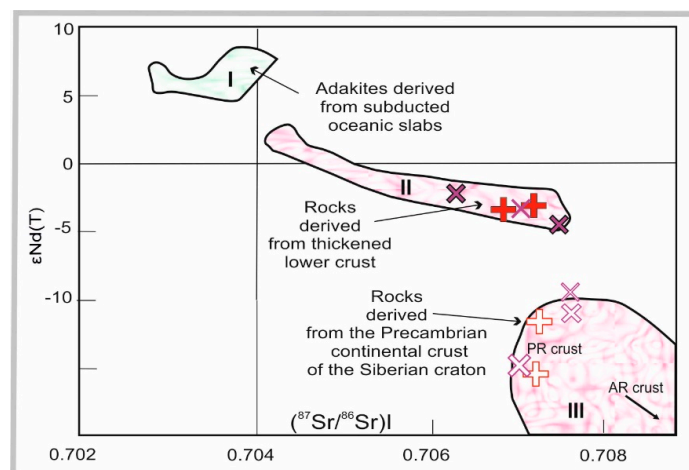


Figure 5. The location of the granitoids of the EF MOOB framing on the diagram of the ratio $(^{87}\text{Sr}/^{86}\text{Sr})_t - \epsilon\text{Nd}(t)$. Fields of adakite derivatives from the subduction oceanic slab according to the [32–34] -I; continental lower crust according to [35–39] -II; the Precambrian continental crust of the Siberian craton-the Aldan shield according to [40] -III. See the legend in Figure 3.

The area of development of rocks of the adakite series in the northern framing of the EF MOOB is confined to the territory of development of Supracrustal Precambrian DSS

complexes (Figure 1b). Their structure is dominated by biotite and garnet-hypersthene, biotite-garnet, two-pyroxene gneiss and schist, quartz amphibolites, quartzites. These complexes are characterized by increased rock content of the main composition (up to 40%) and multiphase high-pressure granulite metamorphism [41,42].

In the petrogenic diagram (Figure 3a), the figurative points of all granitoids are concentrated in the field of I-type granites. The compositions of granitoids correspond to unfractionated rocks of I-, M-, and S-types, and only single values correspond to fractionated granitoids (Figure 3b). Classical adakites [43] are considered rocks with a high Sr/Y ratio and with high concentrations of Sr (>540 ppm), Al₂O₃ (more than 15 wt.%), LREEs, with low Y (<15 ppm) and HREE contents, in the absence of obvious negative Eu anomalies, with low MgO, Ni, and Cr contents. The geochemical characteristics of the considered granitoids of the southern and northern frames of the EF MOOB correspond to the definition of adakites. This is confirmed by the location of the imaging points of these rocks on the classification diagrams of Sr/Y–Y [43] and (La/Yb)_n–Yb_n [44–46], where they correspond to rocks of the adakite series (Figure 6).

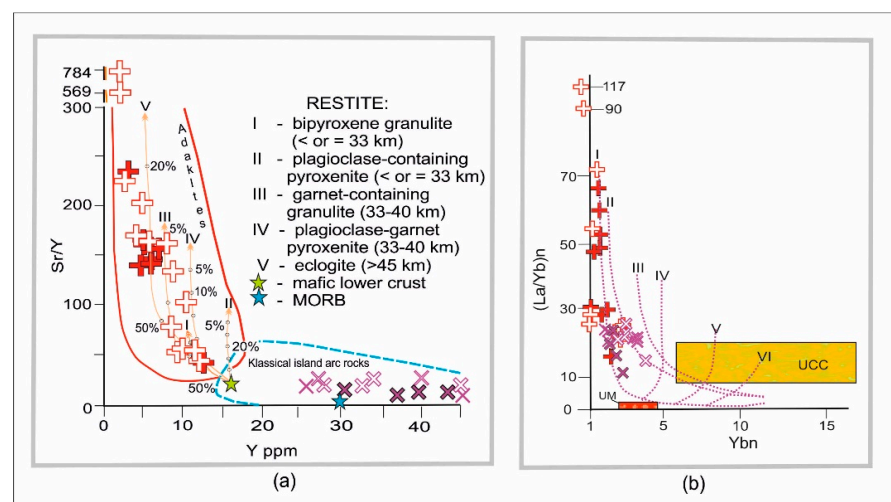


Figure 6. The position of the granitoids on the diagrams: (a) Sr/Y–Y [43–46]. Partial melting curves were calculated for the periodic melting of mafic rocks of the lower crust North China Craton from [47]. (b) the relations (La/Yb)_n–(Yb)_n according to [48] with the outlined trends of source melting according to [49]: I-quartz eclogites; II-garnet amphibolites; II-amphibolites; IV-garnet-containing mantle, with a garnet content of 10%; V-a garnet-bearing mantle, with a garnet content of 5%; VI-garnet-containing mantle, with a garnet content of 3%. UM-upper mantle; UCC-upper continental crust. See the legend in Figure 3.

According to the ratio of petrogenic and rare elements (Figure 7), the figurative dots of these granitoids also fall into the field of high-silica adakites.

According to experimental data [50,51], melting of biotite gneisses and quartz amphibolites at pressures over 12.5 kbar creates conditions for the presence of garnet in the residual phase. It was established by modeling [52] that at the partial melting of slab, adakite magmas can be formed at the depths of 25 to 90 km, at the pressure below the garnet stability (6–28 kbar) and at the temperature from 650 to 1050 °C.

The researched granitoids of the adakite series were formed at the depth of 45–50 km (Figures 6b and 8), which corresponds to the pressure of no more than 13 kbar. A necessary condition for high-silica adakites generation is a high pressure (greater than or equal to 10–12 kbar) and the balance of the melt with garnet-containing restite (Figure 6a,b). Therefore, one can assume with a high degree of certainty that their formation took place in a subduction environment, and the melting was subjected to highly metamorphosed both lower crustal and upper crustal Precambrian formations or delaminated garnet-containing

lower continental crust. Thus, both mantle and crustal matter took part in the composition of the source of the ancestral melts of these rocks.

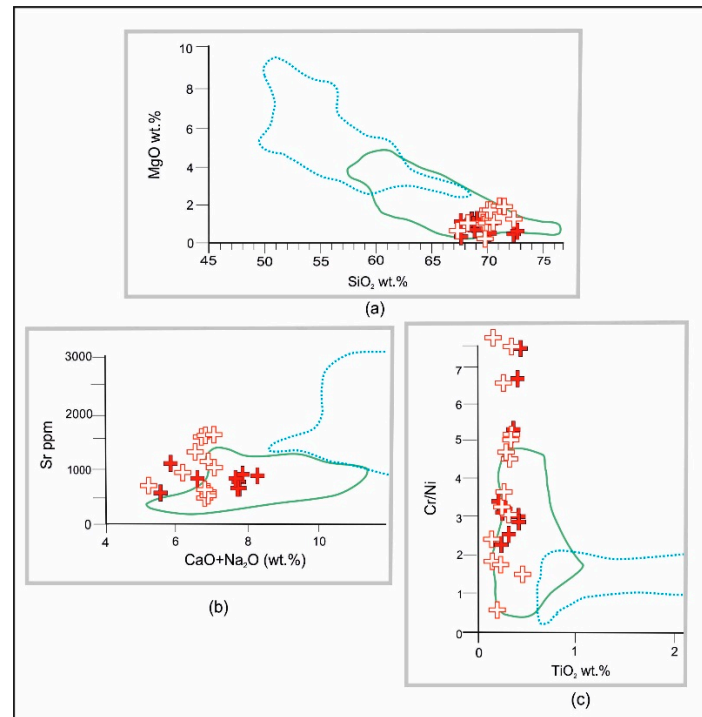


Figure 7. The location granitoids of the adakite series of the EF MOOB framing on the correlation diagrams [46]: (a) MgO – SiO₂; (b) Sr – CaO + Na₂O; (c) Cr/Ni – TiO₂. Solid line—high siliceous adakites; dotted line—low-silica adakites. See the legend in Figure 2.

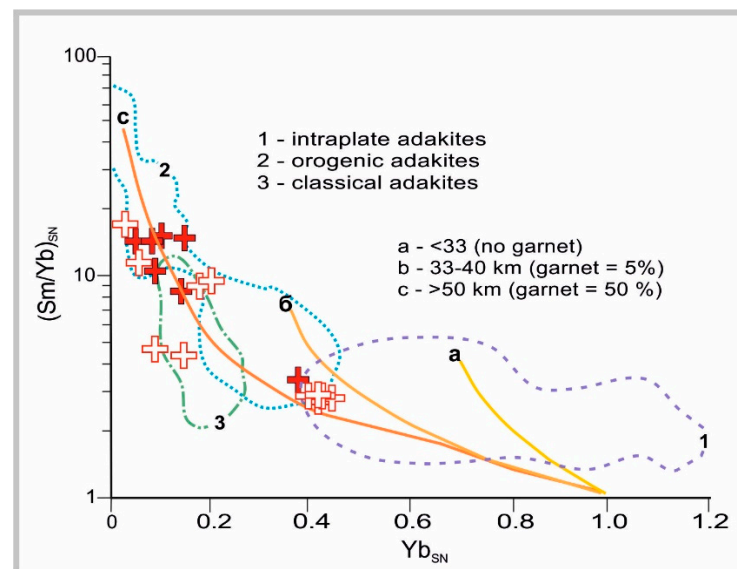


Figure 8. The location of granitoids of the adakite series of the EF MOOB framing on the diagram (Sm/Yb)_{SN}–Yb_{SN} [45]. The position of intraplate adakites (1)–represented by Mesozoic continental adakite rocks of the Northern China craton; orogenic adakites (2)–represented by adakites of the Central Andes, the Tibetan plateau and the Dabie orogen; classical adakites (3). Elements are normalized to the composition of MORB according to [53]. See the legend in Figure 2.

3.1.3. Magmatism of the Second Stage Framed by EF MOOB (140–122 Ma): Differentiated Calc-Alkaline Complexes

The formation of rocks of the adakite complex in the northern and southern frames of the EF MOOB was replaced by the formation of rocks of differentiated calc-alkaline complexes. The complexes are represented mainly by plutonic formations in the northern frames. In the southern frame these complexes are widely presented by volcanogenic rocks (Figure 1b). The explanation of this fact is covered in the varying degree of erosion of these territories. There are three interrelated complexes: plutonic (140–128 Ma), hypabyssal (130–124 Ma), and volcanic (128–122 Ma) [6–12,19], data of the author.

1. Plutonic formations of differentiated calc-alkaline complexes (140–128 Ma).

Rocks of the plutonic complex of granite-granodiorite composition form large batholiths with an area of up to 500 km² or more, small bodies of complex and dike-like shape (Figure 1b). They are presented granodiorites, granites, and quartz diorites (Figure 9a). The rocks belong to the formations of the calc-alkaline series with a ratio of Na₂O/K₂O = 0.9–1.6 (Figure 9c). The total amount of alkalis is almost constant for all varieties (6.1–7.1 wt.%), the content of K₂O = 2.3–3.3, and Na₂O = 3.1–4.1 wt.%. These are mainly high-potassium formations (Figure 9b) of the aluminous series at ASI = 0.9–1.2. They are characterized by moderate-low titanium. According to the isotopic and geochemical characteristics, the rocks belong to the negative εNd-type with εNd(T) = (−2.1)–(−14.6). The isotopic strontium ratios are: ⁸⁷Sr/⁸⁶Sr = 0.7063–0.7075 [6–10] (Figure 5). Isotopic age determined by the ⁴⁰Ar/³⁹Ar and U/Pb methods [6–9,11,12], unpublished data of the author, corresponds to 140–128 Ma, which is confirmed by geological data: the relationship with the enclosing rocks.

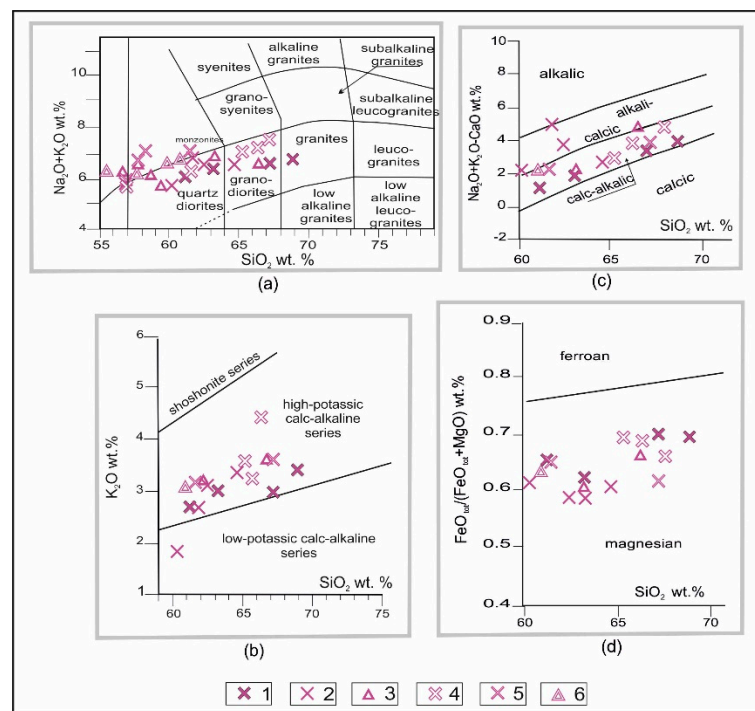


Figure 9. Petrochemical characteristics of igneous rocks of the calc-alkaline series of the EF MOOB framing on classification diagrams: (a) (Na₂O + K₂O) – SiO₂ [25]; (b) K₂O – SiO₂ [26]; (c) (Na₂O + K₂O – CaO) – SiO₂ and (d) FeO_{tot}/(FeO_{tot} + MgO) – SiO₂ by [27]. Legend: of southern framing-plutonic granitoids (1), hypabyssal granitoids (2), volcanoes (3); of northern framing-plutonic granitoids (4), hypabyssal granitoids (5), volcanoes (6).

2. Hypabyssal formations of differentiated calc-alkaline complexes (130–124 Ma).

The formation of the hypabyssal granitoids of monzodiorite-granodiorite composition are shifted in their formation period: 130–124 Ma [6–12], unpublished data of the author. They form large-area laccoliths and lopoliths (up to 200 km²) composed by porphyritic quartz diorites, monzonites, quartz monzonites, and granodiorites (Figure 9a). The rocks belong to the high-potassium calc-alkaline series at $\text{Na}_2\text{O}/\text{K}_2\text{O} = 0.9\text{--}2.2$ (Figure 9b,c). They are characterized by almost unchangeable concentrations of Al_2O_3 (15.1–16.1 wt.%) at $\text{ASI} = 1.1\text{--}1.3$. Granitoids belong to the potassium-sodium series, moderately magnesian (Figure 9d), moderately titanitic. According to the isotope-geochemical characteristics, they also belong to the negative ϵNd -type with $\epsilon\text{Nd}(\text{T}) = (-3.6) - (-4.7)$. The isotopic strontium ratios are $^{87}\text{Sr}/^{86}\text{Sr} = 0.7045\text{--}0.7073$ [6–12] (Figure 5). Geochronological dating of $^{40}\text{Ar}/^{39}\text{Ar}$ and Rb/Sr methods [6–12], author data, indicates that the formation of rocks of this complex occurred in the range of 130–124 Ma.

3. Volcanic formations of differentiated calc-alkaline complexes (128–122 Ma).

Hypabyssal granitoids are comagmates of volcanic formations with the age of 128–122 Ma [6–12] with which they form a single volcano-plutonic complex. Paleovolcanoes of the central type form the rocks of this complex. They are represented by andesitic basalts, andesites, trachyandesite, dacitic andesites, dacites, their tuffs, tufoaleurolites, and tuff sandstones (Figure 9a). According to the petrochemical features, volcanites belong to predominantly sodium alkalinity type rocks: $\text{Na}_2\text{O}/\text{K}_2\text{O} = 0.81\text{--}2.66$, with the total amount of alkalis from 4.6 to 6.9 wt.%. These formations belong to the calc-alkaline series (Figure 9c) from low- to high-potassium varieties (Figure 9b), moderate- to low-titanium; moderate- to high-magnesium (Figure 9c). The alumina content varies from moderate to high with $\text{ASI} = 1.0\text{--}1.3$. Their isotopic and geochemical characteristics are comparable with those of plutonic and hypabyssal granitoids. Volcanites belong to the negative ϵNd -type with $\epsilon\text{Nd}(\text{T}) = (-2.7) - (-3.8)$ at a ratio of $^{87}\text{Sr}/^{86}\text{Sr} = 0.7050\text{--}0.7078$ [6–10]. Determining the age of volcanites by the $^{40}\text{Ar}/^{39}\text{Ar}$ method establishes the period of their formation as 128–122 Ma [6–12], data of the author.

A hollow oblique shape is detected on chondritic normalized graphs (Figure 4a), with almost no Eu anomaly ($\text{Eu}/\text{Eu}^* = 0.7\text{--}0.91$). The predominance of LREEs over HREEs is clearly expressed, and the formations of hypabyssal and volcanic complexes are more enriched with light and intermediate lanthanides ($(\text{La}/\text{Yb})_n = 17.59\text{--}33.04$) than plutonic granitoids ($(\text{La}/\text{Yb})_n = 10.42\text{--}19.17$). The concentration of HREEs in these complexes is contained in absolutely equal amounts. This indicates an increase in the degree of differentiation of REEs from deeper to hypabyssal and volcanogenic formations. The rocks are significantly depleted by Nb, Ta, Ti, Y, Yb and enriched with Rb, Th, K (Figure 4b). The rocks composing plutonic correspond with I-type granites, while the figurative dots of fewer deep formations are shifted to S-type trend (Figure 3a). A regular increase in the ASI value (from 0.9 in plutonic to 1.3 in hypabyssal) and the values of the primary isotopic strontium ratios may indicate an increase in the role of the crustal component in this direction.

It can be stated that differentiated calc-alkaline plutonic-volcano-plutonic complexes with homogeneous geochemical characteristics are formed in the interval of 140–122 Ma [8–14] (data of the author). This indicates the unity of the geodynamic conditions of their formation.

4. Discussion

The oncoming movement of the Siberian and North China cratons in the Late Mesozoic provoked the closure of the MOB. The stages of this process are recorded by the accompanying magmatic events. These events occurred synchronously in the northern and southern frames of the EF MOOB and are most likely associated with the subduction of MOB sediments in both the northern and southern directions (Figure 11). It is reasonable to assume that by the end of the Late Mesozoic, all the igneous rocks described by the author were equidistant from the assumed subduction boundaries (Figure 1c). In this case, the

position of the SSS at that time did not correspond to the current state. Most likely, the SSS wedged between the MOOB and the southern frame of the Siberian craton (DSS) after the completion of all Late Mesozoic magmatism (Figure 1b). As a result of this process, the western part of the area of distribution of magmatic complexes associated with the initial and active phase of subduction of the MOB oceanic crust under the northern frame of the DSS was removed from the body of the belt itself.

The EF MOOB borders on the eastern flank of the SSS along the North-Tukuringra Fault (Figure 1b). The fault zone is 800 km long and up to 50 km wide. In the structure of this structure, tectonically processed sedimentary and volcanic rocks are established. They were previously metamorphosed in the amphibolite facies. Geochronological (U-Pb) and isotope-geochemical (Sm-Nd) studies of these rocks [18] showed that there are metavolcanites with an age of 193 ± 1 Ma; granitoids with an age of 370 Ma. According to the values of $tNd(DM)$, the metamorphic rocks established within the fault zone are divided into rocks with $tNd(DM) = 1.1\text{--}1.9$ and $tNd(DM) = 2.5\text{--}3.1$ Ga. The authors emphasize that the spatial distribution of formations with Late Archean and Proterozoic $tNd(DM)$ values has not been established. Based on the obtained results [18], the authors stated: (1) rocks of different ages are present in the fault zone; (2) this is a zone of tectonic mélangé filled with metamorphosed rocks from the Early Precambrian to the Mesozoic; (3) the formation of the zone occurred in the Mesozoic as a result of Late Jurassic–Early Cretaceous collisional processes. The latter fact is refuted by the finds of Mesozoic rocks within the studied zone. This is evidence that the zone of tectonic mélangé was formed in the post-Mesozoic time.

In the north, the SSS is separated from the DSS by the tectonic zone of the Dzheltulak Fault (Figure 1b). Mylonites, blastomylonites, blastocataclazites, areas of layered rock shale, and silicic-alkaline metasomatism are widely developed within this zone. Using the U-Pb method, it was found that in the zone of the Dzheltulak fault there are formations with an age of 1960–1930, 1750–1700, 1600–1500 Ma (according to zircons), 2000–1350 Ma (according to pyrochlores) [54]. Northeast of the Dzheltulak fault, the above-described Late Jurassic–Early Cretaceous volcano-plutonic complexes are widely manifested (Figure 1b).

A heterogeneous stratification of the structure of the lithosphere was established at the base of the SSS [13–15]. This fact indicates that within the studied territory, horizontal movements occurred in the earth's crust and near-surface space. Within the Dzheltulak zone, there are deeply inclined tectonic boundaries of both modern and earlier formation. The modern (Late Cenozoic) boundaries dip southward, and the paleoboundaries dip northward. It can be assumed that the paleoboundaries of the northern dip arose as a result of Late Mesozoic subduction processes, when the oceanic bed of the MOB subsided under the continental margin of the southern framing of the Siberian craton. Late Cenozoic boundaries may indicate the existence of tectonic rearrangements during this period.

The magmatic complexes accompanying the closure of the EF MOOB were formed almost continuously over time [54]. This is evidence that magmatic and tectonic events occurred throughout the Cretaceous that began with the formation of adakite granitoids. It is shown [32,55,56] that adakite magmatism is associated with the initial stage of the subduction process. It is believed that only at an orthogonal subduction angle, melting of the oceanic crust and its interaction with the overlying mantle and the continental crust are possible [57]. In this case, highly metamorphosed Lower Crustal Precambrian formations in both the northern and southern framing were subjected to melting. The main heat input could occur due to the contact of the oceanic plate with the hot asthenosphere. The increase in heat flow can be explained by the mechanical characteristics and age of the submerged subducting plate. The age of the oceanic plate at that time was no more than 25 Ma. Low Y-Yb contents and high Sr/Y and La/Yb ratios in the studied rocks may indicate the initial slab melting. At the same time, the melts, rising to the surface, passed through highly metamorphosed Precambrian formations. This contributed to the formation of high-silica adakites. The participation of magmatic subduction material in the formation of granitoids of the studied complexes is confirmed by the Th/La– ϵ Sm/La ratio (Figure 10a).

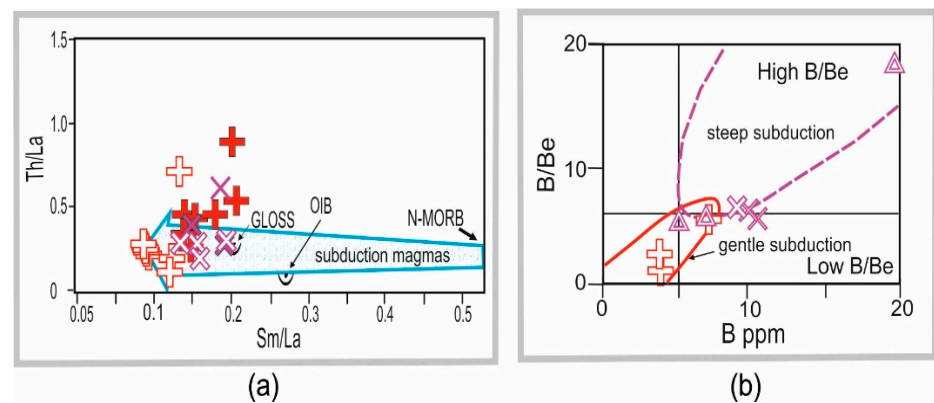


Figure 10. Tectonic interpretation of the EF MOOB framing granitoids based on the taxonomy of the ratio: (a) Th/La–Sm/La. Trend of subduction magmas according to [58], OIB and N-MORB values, according to [31], GLOSS-is the average composition of subduction sediments according to [59]; (b) B/Be–B according to [60].

According to [60], one of the most sensitive indicators of subduction is the mobile boron. Rocks with a high La/Yb ratio and a low Yb concentration (Figure 6b) can be considered as derivatives of slab melting under subduction conditions if they are characterized by low B/Be ratios combined with a high Nb/Ta value. For adakite granitoids, these values are $B/Be = 0.75\text{--}5$; $Nb/Ta = 10\text{--}25$. The values of the B–B/Be ratio also characterize the subduction architecture (Figure 10b). They indicate an initially relatively gentle immersion of the oceanic plate (Figure 11).

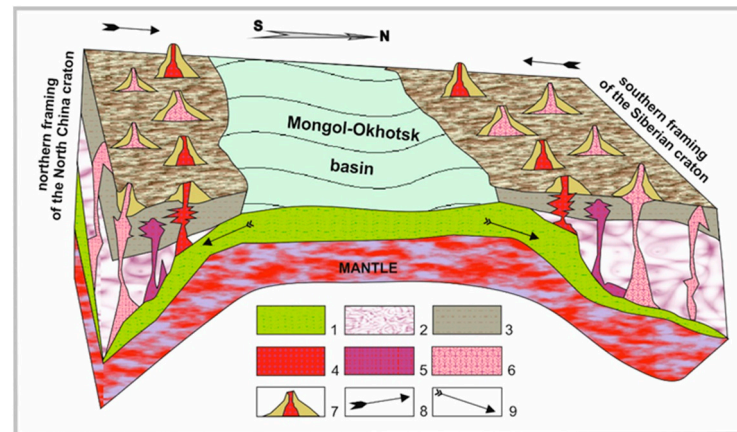


Figure 11. Schematic diagram showing the synchronous subduction of the Mongol-Okhotsk oceanic plate in the northern (under the southern framing of the Siberian Craton) and southern (under the northern framing of the North China Craton) directions in the interval 149–122 Ma. Legend: Oceanic crust (1). Metasomatized mantle (2). Continental crust (3). Magmatic complexes (4–6): adakite series, 149–138 Ma (4), calc-alkaline series-plutonic, 140–128 Ma (5) and volcano-plutonic, 130–122 Ma (6). Volcanoes (7). The direction of movement of cratons (8). The direction of movement of the oceanic crust (9).

The subduction processes caused by the counter motion of the Siberian and North China cratons proceeded according to the “interlocking scissors” principle [61], which corresponds to oblique subduction. It is likely that adakitic granites could have been formed by contact with the hot asthenosphere of the lateral parts of the oceanic plate in subduction “windows”. They usually form during oblique subduction (Figure 11). According to the B/Br–B ratio (Figure 10b), the initial stage of subduction was characterized by a gentle steep subsidence of the oceanic plate. This fact is confirmed by geophysical observations [13–15].

With further subduction, the oceanic plate took a steeper flatter position (Figure 10b), which was accompanied by the formation of differentiated calc-alkaline complexes (Figure 11). A similar point of view on the formation of igneous complexes in the southern framing of MOOB (south-east of the territory under consideration) was expressed in [62,63]. The authors describe a large igneous province of the Greater Xin'an Range, which formed 150–110 Ma ago. The work [62] notes the wide occurrence of adakite rocks. The rocks of the calc-alkaline series are less common here and are replaced by formations with within-plate geochemical features. The author of [62] proposed a subduction model of the Late Mesozoic evolution of the Mongol-Okhotsk orogen. In [63], the authors distinguish four magmatic stages. At the first-initial stage (155 million years ago), rocks are formed, the geochemical characteristics of which make it possible to compare them with the rocks of the adakite series. According to the authors of [63], adakitic magmatism changed to calcalkaline, which continued in this area until 126 Ma ago. Researchers also associate all these events with subduction processes [63]. The work [16] presents a diagram of the change in time of the position of the observation point 52°N–117°E a.s.l. within EF MOOB based on paleomagnetic data. According to this diagram, subduction processes in the region begin about 150 Ma ago, and the collisional stage, about 120 Ma ago. This was reflected in the described magmatic events: suprasubduction rocks in the studied area begin to form at about 150 (149) Ma, and bimodal collisional formations, from 120 (119) Ma. The geochronological results obtained by researchers in China (the igneous province of the Greater Xin'an Range) [62,63] confirm that the closure of the MOOB occurred sequentially and provoked a change in geodynamic settings: from subduction to collisional.

5. Conclusions

Comparative analysis of magmatic events in the frame of the WF MOOB showed the following:

1. In the interval of 149–138 Ma, granitoids were formed comparable in their material characteristics to the rocks of the adakite series. What is typical for the initial stage of subduction processes. In the range of 140–122 Ma, suprasubduction rocks of the calc-alkaline series begin to form. The formation of these formations occurred both in the northern and southern framing of the belt at the same time.
2. The material composition of rocks reflects not only the specifics of the continental crust, which was involved in melting during their formation, but also the architecture of subduction processes.
3. In this case, it was a synchronous subduction: the oceanic crust of the MOB subsided under the southern edge of the Siberian Craton and the northern edge of the North China Craton. These processes marked the beginning of the final closure of the Mongolian-Okhotsk basin and the formation of an orogen.

Funding: This research was carried out with partial financial support from the Russian Foundation for Basic Research (Grant No. 13-05-12043-ofi-m). Most of the research was carried out without received no external funding.

Data Availability Statement: Supporting data are in my published works, they are in the list of references.

Acknowledgments: The author is grateful to the staff of the IGeP FEB RAS E.V. Ushakova and A.A. Zenevich; to the staff of IGEM RAS A.V. Chugaev, T.I. Oleinikova, who carried out analytical studies of the rocks.

Conflicts of Interest: The authors declare no conflict of interest.

References

1. Khanchuk, A.I. (Ed.) *Geodynamics, Magmatism and Metallogeny of the Russian East*; Book 1; Dalauka Press: Vladivostok, Russia, 2006; p. 572.
2. Parfenov, L.M.; Popeko, L.I.; Tomurtogoo, O. The problems of tectonics of the Mongol-Okhotsk orogene. *Russ. J. Pac. Geol.* **1999**, *18*, 24–43.
3. Krasnyi, L.I.; Peng, Y.B. (Eds.) *Geological Map of Amur Region and Adjacent Scale 1:2,500,000*; Roskomnedra: Blagoveshchensk, Russia; VSEGEI: Sankt-Petersburg, Russia; MG&MR: Harbin, China, 1996.
4. Natalin, B.A. Mesozoic accretion and collision tectonics of the Far East south of the USSR. *Russ. J. Pac. Geol.* **1991**, *5*, 3–23.
5. Derbeko, I.; Kichanova, V. Post-Mesozoic Evolution of the Eastern Flank of the Mongol–Okhotsk Orogenic Belt. In *Advances in Geophysics, Tectonics and Petroleum Geosciences*; Springer: Cham, Switzerland, 2022; pp. 577–581. [[CrossRef](#)]
6. Kozyrev, S.K.; Volkova, Y.R.; Ignatenko, N.N. *State Map of the Russian Federation-Scale 1: 200 000*; Series Zeya; Sheet N-51-XXIV; Explanatory note; Chepygin, V.E., Ed.; Moscow branch of FSBI“VSEGEI”: Moscow, Russia, 2016.
7. Kozyrev, S.K.; Volkova, Y.R.; Ignatenko, N.N. *State Map of the Russian Federation-Scale 1: 200 000*; Series Zeya; Sheet N-51-XXIII; Explanatory note; Chepygin, V.E., Ed.; Moscow branch of FSBI“VSEGEI”: Moscow, Russia, 2016.
8. Larin, A.A.; Kotov, A.B.; Salnikova, E.B.; Kovach, V.P.; Sergeeva, N.A.; Yakovleva, S.Z. Mesozoic granites of the Chubachinsky massif of the Tukuringra complex (Dzhugdzhur-Stanovaya folded region): New geochemical, geochronological and isotope-geochemical data. *Petrology* **2001**, *9*, 417–432.
9. Antonov, A.Y. *Geochemistry and Petrology of Meso-Cenozoic Magmatic Formations and Mantle Diapirism*; Academic Publishing House Geo, Ltd.: Novosibirsk, Russia, 2008; p. 250.
10. Strikha, V.E. *Mesozoic Granitoids of Gold-Bearing Regions of the Upper Amur Region*; AmSU Publishing House: Blagoveshchenck, Russia, 2012; p. 188.
11. Timashkov, A.N.; Shatova, N.V.; Berezhnaya, N.G.; Balashova, Y.S.; Morozova, A.B.; Lvov, P.A.; Shokalsky, S.P.; Plekhanov, A.O.; Molchanov, A.V.; Radkov, A.V. Geochronological studies of granitoids of the Stanovoi folded region. *Reg. Geol. Metallog.* **2015**, *61*, 35–50.
12. Sorokin, A.A.; Ponomarchuk, V.A.; Kozyrev, S.K.; Sorokin, A.P.; Voropaeva, M.S. Geochronology and correlation of Mesozoic magmatic formations of the Northern edge of Amur superterrains. *Stratigr. Geol. Correl.* **2004**, *12*, 36–52.
13. Didenko, A.N.; Efimov, A.S.; Nelyubov, P.A.; Salnikov, A.S. Structure and evolution of the Earth’s crust in the region of junction of the Central Asian fold belt and the Siberian platform: Skovorodino–Tomot profile. *Russ. J. Geol. Geoph.* **2013**, *54*, 1236–1249. [[CrossRef](#)]
14. Didenko, A.N.; Kaplun, V.B.; Malyshev, Y.F.; Shevchenko, B.F. Lithospheric structure and mesozoic geodynamics of the Eastern Central Asian orogen. *Russ. J. Geol. Geoph.* **2010**, *51*, 492–506. [[CrossRef](#)]
15. Shevchenko, B.F.; Popeko, L.I.; Didenko, A.N. Tectonics and evolution of the lithosphere of the eastern fragment of the Mongol-Okhotsk orogenic belt. *Geodyn. Tectonoph.* **2014**, *5*, 667–682. [[CrossRef](#)]
16. Zhang, K.-J.; Yan, L.-L.; Chen, J. Switch of NE Asia from extension to contraction at the mid-Cretaceous: A tale of the Okhotsk oceanic plateau from initiation by the Perm Anomaly to extrusion in the Mongol–Okhotsk ocean? *Earth Sci. Rev.* **2019**, *198*, 102941. [[CrossRef](#)]
17. Bouysse, P. Geological Map of the World, Scale 1:50 000 000. 2009. Available online: <http://www.ccgm.org> (accessed on 22 August 2022).
18. Velikoslavinsky, S.D.; Kotov, A.B.; Salnikova, E.B.; Larin, A.M.; Sorokin, A.A.; Sorokin, A.P.; Kovach, V.P.; Tolmacheva, E.V.; Yakovleva, S.Z.; Anisimova, I.V. On the age of the Ustygilyuya stratum of the Mill Selenga-Stanovoy superterrane complex of the Central Asian fold belt. *Dokl. Earth Sci.* **2012**, *444*, 402–406.
19. Derbeko, I.M.; Agafonenko, S.G.; Kozyrev, S.K.; Vyunov, D.L. The Umlekan-Ogodzha volcanic belt (the problem bodily separation). *Lithosphere* **2010**, *3*, 70–77.
20. Derbeko, I.M.; Ponomarchuk, V.A.; Chugaev, A.V.; Travin, A.V.; Ponomarchuk, A.V. Correlation of the andesite complexes of the southern edge of Mongol-Okhotsk orogenic belt Eastern frame according to its geochronological, geochemical and isotope-geochemical data. *Russ. J. Geol. Geoph.* **2020**, *61*, 1109–1120. [[CrossRef](#)]
21. Derbeko, I.M. Bimodal volcano-plutonic complexes in the frames of Eastern member of Mongol-Okhotsk orogenic belt, as a proof of the time of final closure of Mongol-Okhotsk basin. In *Updates in Volcanology—A Comprehensive Approach to Volcanological Problems*; Stoppa, F., Ed.; InTech: Rijeka, Croatia, 2012; pp. 99–124.
22. Derbeko, I.M.; Markevich, V.S. Late Mesozoic subalkali volcanism of the south framing of the eastern link of Mongol-Okhotsk orogenic belt. *Nat. Tech. Sci.* **2013**, *2*, 135–143.
23. Derbeko, I.M.; Chugaev, A.V. Late Mesozoic adakite granites of the southern frame of the eastern flank of the Mongol-Okhotsk orogenic belt: Material composition and geodynamic conditions of formation. *Geodyn. Tectonophys.* **2020**, *11*, 474–490. [[CrossRef](#)]
24. Derbeko, I.M. Mesozoic adakite volcano-plutonic complex of the Upper Amur region (Russia). In *Petrography of Igneous and Metamorphic Rocks*; Golubev, A.I., Shchiptsov, V.V., Eds.; Karelian Scientific Center of the Russian Academy of Sciences: Petrozavodsk, Russia, 2015; pp. 153–155.
25. Bogaticov, O.A. *Magmatic Rocks*; Nauka: Moscow, Russia, 1983; p. 367.
26. Le Bas, M.; Le Maitre, R.W.; Streckeisen, A.; Zanettin, B. A chemical classification of volcanic rocks based on the total-silica diagram. *J. Petrol.* **1986**, *27*, 745–750. [[CrossRef](#)]

27. Frost, B.R.; Barnes, C.G.; Collins, W.J.; Arculus, R.G.; Ellis, D.J.; Frost, C.D. A geochemical classification for granitic rocks. *J. Petrol.* **2001**, *42*, 2033–2048. [[CrossRef](#)]
28. Zen, E.-A.N. Aluminum enrichment in silicate melts by fractional crystallization: Some mineralogic and petrographic constraints. *J. Petrol.* **1986**, *27*, 1095–1117. [[CrossRef](#)]
29. Chappell, B.W.; White, A.J.R. I- and S-type granites in the Lachlan Fold Belt. *Trans. R. Soc. Edinb.* **1992**, *83*, 1–26.
30. Whalen, J.B.; Currie, K.L.; Chappell, B.W. A-Type Granites—Geochemical Characteristics, Discrimination and Petrogenesis. *Contrib. Mineral. Petrol.* **1987**, *95*, 407–419. [[CrossRef](#)]
31. Sun, S.-S.; McDonough, W.F. Chemical and isotopic systematics of oceanic basalts: Implications for mantle composition and processes. In *Magmatism in the Ocean Basins*; Saunders, A.D., Norry, M.J., Eds.; The Geological Society Special Publication: London, UK, 1989; Volume 42, pp. 313–345. [[CrossRef](#)]
32. Defant, M.J.; Drummond, M.S. Derivations of some modern arc magmas by melting of young subducted lithosphere. *Nature* **1990**, *347*, 662–665. [[CrossRef](#)]
33. Kay, R.W. Aleutian magnesian andesites: Melts from subducted Pacific Ocean crust. *J. Volcan. Geotherm. Res.* **1978**, *4*, 117–132. [[CrossRef](#)]
34. Sajona, F.G.; Maury, R.C.; Bellon, H.; Cotton, J.; Defant, M.J. Initiation of subduction and the generation of slab melts in western and eastern Mindanao, Philippines. *Geology* **1993**, *21*, 1007–1010. [[CrossRef](#)]
35. Muir, R.J.; Weaver, S.D.; Bradshaw, J.D.; Eby, G.N.; Evans, J.A. Geochemistry of the Cretaceous Separation Point Batholith, New Zealand: Granitoid magmas formed by melting of mafic lithosphere. *J. Geol. Soc.* **1995**, *152*, 689–701. [[CrossRef](#)]
36. Petford, N.; Atherton, M. Na-rich partial melts from newly underplated basaltic crust: The Cordillera Blanca Batholith, Peru. *J. Petrol.* **1996**, *37*, 1491–1521. [[CrossRef](#)]
37. Wang, Q.; McDermott, F.; Xu, J.-F.; Bellon, H.; Zhu, Y.T. Cenozoic K-rich adakitic volcanic rocks in the Hohxil area, northern Tibet: Lower-crustal melting in an intracontinental setting. *Geology* **2005**, *33*, 465–468. [[CrossRef](#)]
38. Wen, D.R.; Chung, S.L.; Song, B.; Iizuku, Y.; Yang, H.J.; Ji, J.Q.; Liu, D.Y.; Sylvain, G. Late Cretaceous intrusions of adakitic geochemical characteristics, SE Tibet: Petrogenesis and tectonic implications. *Lithos* **2008**, *105*, 1–11. [[CrossRef](#)]
39. Topuz, G.; Okay, A.I.; Altherr, R.; Schwarz, W.H.; Siebel, W.; Zack, T. Post-collisional adakite-like magmatism in the Agvanis Massif and implications for the evolution of the Eocene magmatism in the Eastern Pontides (NE Turkey). *Lithos* **2011**, *125*, 131–150. [[CrossRef](#)]
40. Bogatkov, O.A.; Kovalenko, V.I. *Types of Magmas and Their Sources in the History of the Earth*; Part 1; Nauka: Moscow, Russia, 2006; p. 395.
41. Karsakov, L.P. Stanovaya folded system, its boundaries, structural-material complexes. In *Modern Tectonic Concepts and Regional Tectonics of the East of the USSR*; Yakutsk branch of the Siberian Branch of the USSR Academy of Sciences: Yakutsk, Russia, 1980; pp. 142–144.
42. Petruk, N.N.; Belikova, T.V.; Derbeko, I.M. *Geological Map of Amur Region. Scale 1:500 000*; Amurgeologiya: Blagoveshchensk, Russia, 2002; p. 263.
43. Defant, M.J.; Jackson, T.E.; Drummond, M.S.; Bellon, H.; Feigenson, M.D.; Maury, R.C.; Stewart, R.H. The geochemistry of young volcanism throughout western Panama and south-eastern Costa Rica: An overview. *J. Geol. Soc.* **1992**, *149*, 569–579. [[CrossRef](#)]
44. Martin, H. The mechanisms of petrogenesis of the Archaean continental crust—comparison with modern processes. *Lithos* **1993**, *46*, 373–388. [[CrossRef](#)]
45. Martin, H. Adakitic magmas: Modern analogues of Archaean granitoids. *Lithos* **1999**, *46*, 411–429. [[CrossRef](#)]
46. Martin, H.; Smithies, R.H.; Rapp, R.; Moyen, J.-F.; Champion, D. An overview of adakite, tonalite-trondhjemite-granodiorite (TTG), and sanukitoid: Relationships and some implications for crustal evolution. *Lithos* **2005**, *79*, 1–24. [[CrossRef](#)]
47. Ma, Q.; Zheng, J.P.; Xu, Y.G.; Griffin, W.L.; Zhang, R.S. Are continental “adakites” derived from thickened or foundered lower crust? *Earth Plan. Sci. Lett.* **2015**, *419*, 125–133. [[CrossRef](#)]
48. Shaw, J.E.; Baker, J.A.; Menzies, M.A.; Thirlwall, M.F.; Ibrahim, K.M. Petrogenesis of the largest intraplate volcanic field on the Arabian Plate (Jordan): A mixed lithosphere–asthenosphere source active by lithospheric extension. *J. Petrol.* **2003**, *44*, 1657–1679. [[CrossRef](#)]
49. Barbarian, B. Granitoids: Main petrogenetic classifications in relation to origin and tectonic setting. *Geo. J.* **1990**, *25*, 227–238. [[CrossRef](#)]
50. Patiño-Douce, A.E.; Beard, J.S. Dehydration -melting of Biotite Gneiss and Quartz Amphibole from 3 to 15 Kbar. *J. Petrol.* **1995**, *36*, 707738.
51. Patiño-Douce, A.E. What do experiments tell us about the relative contributions of crust and mantle to the origin of granitic magmas? In *Understanding Granites: Integrating New and Classical Techniques*; Castro, A., Fernandez, C., Vigneresse, J.L., Eds.; Geological Society: London, UK, 1999; Volume 168, pp. 55–75.
52. Thorkelson, D.J.; Breitsprecher, K. Partial melting of slab window margins: Genesis of adakitic and non adakitic magmas. *Lithos* **2005**, *79*, 25–41. [[CrossRef](#)]
53. Arevalo, R., Jr.; McDonough, W.F. Chemical variations and regional diversity observed in MORB. *Chem. Geol.* **2010**, *271*, 70–85. [[CrossRef](#)]
54. Arkhangelskaya, V.V.; Kazansky, V.I.; Prokhorov, K.V.; Sobachenko, V.N. Geological structure, zoning and formation conditions of the Katuginsky Ta-Nb-Zr deposit, Russian. *Russ. J. Geol. Geoph.* **1993**, *54*, 115–131.

55. Lomize, M.G. The initial phase of subduction on the continental margins. *Geotectonics* **2003**, *5*, 73–88.
56. Avdeiko, G.P.; Palueva, A.A.; Kuvikas, O.V. Adakites in subduction zones of the Pacific ring: Review and analysis of geodynamic conditions of formation. *Bulletin Kamchatka Bering State University. J. Earth Sci.* **2011**, *1*, 45–60.
57. Stern, C.R.; Kilian, R. Role of the subducted slab, mantle wedge and continental crust in the generation of adakites from the Andean Austral Volcanic Zone. *Contrib. Mineral. Petrol.* **1996**, *123*, 263–281. [[CrossRef](#)]
58. Tommasini, S.; Conticelli, S.; Avanzinelli, R. The Th/La and Sm/La conundrum of the Tethyan realm lamproites. *Earth Planet Sci. Lett.* **2011**, *301*, 469–478. [[CrossRef](#)]
59. Plank, T.; Langmuir, C.H. The chemical composition of subducting sediments: Implications for the crust and mantle. *Chem. Geol.* **1998**, *145*, 325–394. [[CrossRef](#)]
60. Mohan, M.; Kamber, B.S.; Piercey, S.J. Boron and arsenic in highly evolved Archean felsic rocks: Implications for Archean subduction processes. *Earth Planet Sci. Lett.* **2008**, *274*, 479–488. [[CrossRef](#)]
61. Zonenshain, L.P.; Kuzmin, M.I.; Natapov, L.M. *Tectonics of Lithospheric Plates in the Territory of the USSR*; Book 1; Nedra: Moscow, Russia, 1990; p. 328.
62. Zhang, K.J. Genesis of the Late Mesozoic Great Xing’an Range Large Igneous Province: A Mongol–Okhotsk slab window model. *Int. Geol. Rev.* **2014**, *56*, 1557–1583. [[CrossRef](#)]
63. Liu, C.; Zhou, Z.; Tang, Y.; Wu, C.; Li, H.; Zhu, Y.; Jiang, T.; Liu, W.; Ye, B. Geochronology and tectonic settings of Late Jurassic—Early Cretaceous intrusive rocks in the Ulanhot region, central and southern Da Xingan Range. *Geol. Mag.* **2017**, *154*, 923–945. [[CrossRef](#)]